

Fabrication and characterization of Zn doped CuO nanofiber using newly designed nanofiber generator for the photodegradation of methylene blue from textile effluent

RAMASAMY GOPALSAMY SETHURAMAN¹, THANGAMUTHU VENKATACHALAM^{2,*},
SELVARAJ DINESH KIRUPHA³

¹Department of Physics, Kumaraguru College of Technology, Coimbatore-641 049, India

²Department of Physics, Coimbatore Institute of Technology, Coimbatore-641 014, India

³Department of Chemistry, Coimbatore Institute of Technology, Coimbatore-641 014, India

High aspect ratio, Zn doped copper oxide (Zn-CuO) nanofibers have been fabricated employing a newly designed electrospun coating unit using copper acetate, sodium hydroxide and polyethylene glycol in aqueous state. The prepared Zn doped copper oxide (Zn-CuO) nanofibers were sintered at 400 °C, 500 °C and 600 °C separately and characterized using X-ray diffraction XRD, Fourier transformation infrared spectroscopy FT-IR, scanning electron microscopy SEM, energy dispersive spectroscopy EDS. The average crystallite size was in the range of 28 nm to 30 nm. Optical properties of Zn-CuO nanofibers were analyzed using UV-DRS studies which showed a blue shift in the absorption band. An increase in band gap with the increase in post-annealing temperature was observed due to the blue shift in absorption edge of CuO causing enhanced photodegradation. The catalytic properties of the CuO nanofibers were tested using methylene blue in aqueous medium. The influences of parameters responsible for high photodegradation were optimized and the rate of the photodegradation process was calculated using photodegradation kinetics. The reusability test was conducted to find the stability of the fabricated Zn-CuO nanofibers.

Keywords: *copper oxide; dopant; nanofiber; electrospinning; band gap; photocatalyst*

1. Introduction

Large surface area, chemical stability and high electron mobility are notable characteristics of transition metal oxides at nanoscale. These properties are due to the quantization effect of bulk material into nanostructured compounds. Among transition metal oxide, CuO is a p-type semiconductor with a narrow band gap of 1.2 eV to 1.7 eV, widely used as a source of charge carriers [1]. It exists in two forms: as cuprous oxide Cu₂O and cupric oxide CuO with excellent properties and promising applications in the field of lithium-ion electrode materials [2], magnetic storage materials [3], gas sensing [4], photocatalysis [5] and solar cells [6]. The physical and chemical properties of nanostructured semiconductor materials are determined through their shape, size and dimensional morphology.

Various strategies have been applied by researchers to optimize such structured compounds for potential applications. One of the most important factors which determines the morphology and causes changes in physical and chemical properties is the fabrication process. Doping is a tailoring method used for changing physicochemical properties of CuO metal oxide by dopants, such as Ce, Ni and Zn, etc. [7, 8]. Zn²⁺ is chosen as an effective dopant since it has almost the same ionic radius and ionic states as Cu (Zn²⁺: 0.074 nm, Cu²⁺: 0.072 nm). As a result, Zn can easily be doped into CuO matrix and produce effective defects in the CuO nanostructures [9]. Post-annealing time is a commonly used optimizing parameter which can cause a change in oxidation state of copper resulting in the change of physical and chemical properties. Xi et al. [10] observed a change in size and morphology from microsphere to nanowires with an increase in post-annealing temperature

*E-mail: tvenkatachalam@cit.edu.in

in synthesized CuO nanowires using hydrothermal method. Sahay et al. [11] observed a change in crystallite size of CuO nanowires with an increase in post-annealing temperature and dwelling time using sol-gel method.

Many synthesizing techniques, hydrothermal [12], electrochemical deposition [13], sol-gel technology [14] and chemical vapour deposition [15] have been used for synthesis of CuO nanomaterials with controlled shape and size. Electrospinning is the most commonly explored method for synthesizing 1D nanostructured materials since it is the simplest, economical and most versatile technique for synthesizing nanofibers with various compositions, uniform diameter and significant length. Electrospinning is a process in which the high voltage is applied to a polymer droplet at the syringe needle tip. Charge built up over the droplet elongates it, which results in formation of a Taylor cone as soon as the charge overcomes the precursor solution surface tension [16].

Large amount of synthetic organic dyes is used in textile, leather, cosmetics, plastics, food and pharmaceutical industries in dyeing process which consumes large amount of water in finishing process [17–23]. The wastewater containing the dyestuff is carcinogenic and mutagenic, is highly stable in light and contains bleaching agents, therefore it should be properly treated before entering into the living environment [24–32]. Among commonly used industrial dyes, methylene blue is considered as a predominant cationic dye used in major industries such as paper, textile, cotton, leather, silk, etc. These industrial effluents cause harmful effects to the plant species since they do not allow the light transmission to the root through wastewater causing disruption in the growth [33–36]. Several methods have been employed for the removal of toxic dyes from wastewater. Adsorption is a widely used method but there are some disadvantages, such as production of secondary effluents and spent adsorbents [37]. Hence, an alternative to minimize the disadvantages faced in adsorption method is the dye effluent treatment which has to be both cost efficient and economical [38–40].

Photocatalysis is considered to be the most effective and economical method used for treating textile dye effluents. Transition metal oxide Zn-CuO, when used as a photocatalyst, has the ability to produce OH^\bullet radicals which play an active role in the degradation of organic dyes.

In the present paper, Zn-CuO nanofiber was fabricated through electrospinning method using lab scale designed nanofiber generator unit. The fabricated Zn doped CuO nanofibers were characterized using spectral techniques to find out the surface/structural morphology, chemical composition and physical nature of this compound. The Zn-CuO nanofiber were annealed at different post-annealing temperatures 400 °C, 500 °C and 600 °C separately. The so prepared Zn-CuO nanofibers were tested as a photocatalyst for the degradation of toxic organic dyes from wastewater in a photodegradation process. The process parameters were optimized and explained in detail. Langmuir-Hinshelwood (L-H) kinetics model was applied to the obtained experimental data, to find the nature, reaction rate and spontaneity of the process. In order to find the stability nature of the Zn-CuO nanofibers, recycling experiments were carried out.

2. Experimental

2.1. Preparation of CuO precursor solution

2 g of copper acetate ($\text{Cu}(\text{CH}_3\text{COO})_2 \cdot \text{H}_2\text{O}$, Sigma-Aldrich), 0.1 g of zinc acetate ($\text{Zn}(\text{O}_2\text{CCH}_3)_2 \cdot (\text{H}_2\text{O})_2$, Sigma-Aldrich) and 1.2 g of sodium hydroxide (NaOH, Merck) were grinded separately in a mortar with a pestle. The obtained fine powders of acetate salts and sodium hydroxide were mixed with 3.6 mL of polyethylene glycol (PEG 400, Sigma-Aldrich) and made into a fine paste. The paste was washed repeatedly with distilled water under magnetic stirring and finally dried in ethanol medium. The obtained pale blue colored paste was sintered at 70 °C in an oven for 2 h and annealed at 400 °C, 500 °C and 600 °C separately for 2 h. The annealed Zn-CuO precursor samples were mixed separately with polyvinyl alcohol (PVA, Sigma-Aldrich) and used for the generation of Zn doped CuO nanofibers.

2.2. Preparation of Zn doped CuO nanofibers

Zn doped CuO precursor was dissolved in ethanol and sonicated for 30 min to get a homogeneous solution. The homogeneous precursor solution was filled in a syringe (fiber producing unit) which was connected with a hypodermic needle (dia. 27) placed inside the designed nanofiber generator unit (Fig. 1).

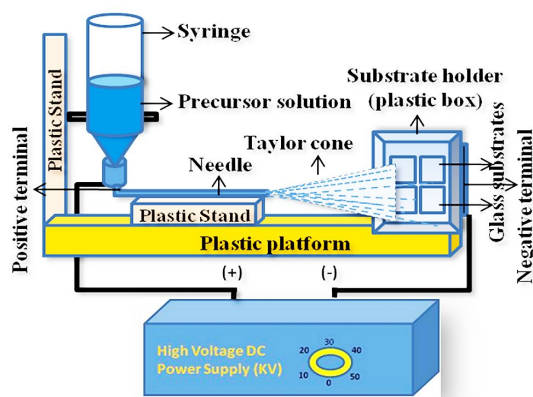


Fig. 1. General outline of designed nanofiber generator.

The designed nanofiber generating unit consists of three major sections: (i) power supply unit based on a microcontroller unit able to generate 0 kV to 30 kV voltage between the needle and the collecting unit; (ii) nanofiber production unit, in which the spinneret solution is fed with a syringe and made to flow through the hypodermic needle to produce droplets. The needle is connected to the positive terminal and the collecting unit is connected to the negative terminal; (iii) nanofiber collector unit with the flow rate of 0.2 mL/h and applied field of 25 kV/cm; a distance of 8 cm is kept between the needle tip and the collector, the droplets formed at the tip of the needle ooze out which results in tailored cones and as a result nanofibers are deposited on four glass substrate plates. The fabricated nanofibers are then collected, covered with lids and subjected to characterization.

2.3. Characterization

The structural and morphological characterizations of the Zn-CuO nanofibers were carried

out with X'Pert PRO, X-ray diffractometer using CuK α radiation ($\lambda = 1.5406 \text{ \AA}$). The surface morphological properties of the nanofibers were characterized using scanning electron microscope (JEOL, JSM) and energy dispersive EDX spectrometry. The optical properties of Zn-CuO nanofibers were studied by measuring UV-reflectance spectra with UV-Vis spectrophotometer (Shimadzu UV-2100) in the range between 200 nm and 800 nm. Fourier transformation analysis of Zn-CuO nanofibers was carried out with Thermal Nicolet 6700, NEXUS. The photoluminescence studies of the prepared Zn-CuO nanofibers were performed using a spectrometer (LABRAM 800) equipped with a He-Cd laser excitation source. The absorbance of methylene blue dye was measured using UV spectrophotometer (Shimadzu UV-3600).

3. Results and discussion

3.1. Characterization of Zn-CuO nanofibers

The XRD patterns of post-annealed Zn doped CuO nanofibers were recorded in the 2θ range of 10° to 80° and are presented in Fig. 2.

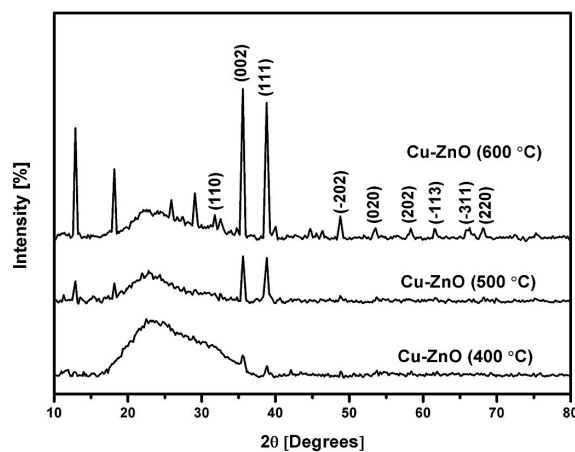


Fig. 2. XRD patterns of Zn-CuO nanofibers post-annealed at different temperatures.

The sharp peaks with high intensity show the crystalline nature of Zn-CuO nanofibers. The peaks observed at 32.29° (1 1 0), 35.35° (-1 1 1), 38.55°

(1 1 1), 48.61° (-2 0 2), 53.20° (0 2 0), 58.16° (2 0 2), 61.29° (-1 1 3), 66.17° (-3 1 1) and 67.77° (1 1 3) correspond to the monoclinic structure of Zn doped CuO nanofibers (space group C_2/c). With an increase in the post annealing temperature, the diffraction peaks get broadened due to the reduction of crystallite size of the Zn-CuO nanofiber. The crystallite sizes of the nanofiber were calculated using Scherrer equation:

$$D = \frac{0.94\lambda}{\beta \cos\theta} \quad (1)$$

where D is the crystallite size, λ is the wavelength (1.546 \AA for $\text{CuK}\alpha$), β is the full-width at half-maximum (FWHM) of intensity peak after subtracting the equipment broadening and θ is the diffraction angle. The relation for strain is:

$$\varepsilon = \frac{\beta \cot\theta}{4} \quad (2)$$

A graph showing crystallite size and lattice strain as a function of post-annealing temperature is shown in Fig. 3.

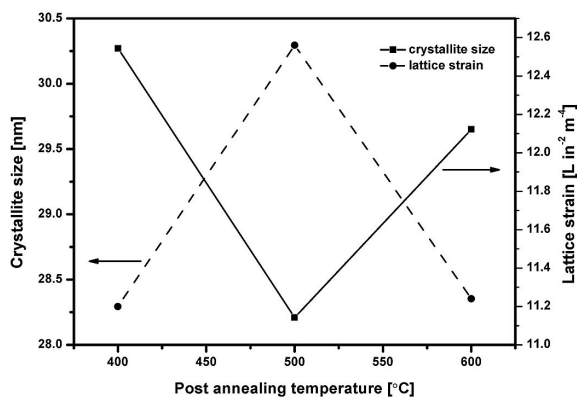


Fig. 3. Crystallite size and lattice strain as a function of post annealing temperature.

As expected, the lattice strain increases with a decrease in crystallite size of the Zn-CuO nanofiber. Furthermore, the sharp intense peaks at $2\theta = 35.46^\circ$, 42.12° corresponding to Zn dopant addition grow higher with the increase in the post annealing temperature, indicating the incorporation of Zn^{2+} into CuO lattice which corresponds to the JCPDS Card No. 41-1442. Since the atomic

radii of Zn^{2+} (0.074 \AA) and Cu^{2+} (0.073 \AA) are very similar, hence Zn^{2+} has been successfully incorporated without causing any changes to the parent CuO matrix. The crystallite sizes of post-annealed Zn-CuO nanofibers were calculated using Scherrer equation and are presented in Table 1, along with lattice strain and other parameters calculated from the XRD images.

The surface morphology of the post-annealed Zn-CuO nanofibers was analyzed using SEM micrographs presented in Fig. 4. The samples of Zn-CuO nanofibers post-annealed at 400°C , 500°C and 600°C are shown separately along with their EDX analysis results. From the SEM micrographs observations, it is clear that the Zn-CuO nanofibers show clusters of agglomeration of particles with cylindrical shape. With an increase in temperature, agglomeration of Zn^{2+} over the CuO matrix can be observed clearly. Incorporation of Zn^{2+} into CuO matrix results in molecular structural disorder and lattice strain causing clustering of nanostructures. The EDX results show the presence of Zn^{2+} , Cu^{2+} along with oxygen O suggesting the formation of mixed metal oxide formation. The presence of Si atom is due to the collector plate. The percentage composition of elements present in each post-annealed Zn-CuO nanofiber sample are presented in Table 2.

The FT-IR spectra of the post-annealed Zn-CuO nanofibers are presented in Fig. 5.

From the observations, the band between 400 cm^{-1} to 700 cm^{-1} corresponds to the metal oxide bond [41]. The bands positioned at 531 cm^{-1} and 533 cm^{-1} correspond to the Cu-O stretching vibrations. The other characteristic peaks representing polycrystalline nature of CuO nanofibers are positioned at 487 cm^{-1} , 484 cm^{-1} , 481 cm^{-1} and 483 cm^{-1} , respectively. The broad peak at 3490 cm^{-1} corresponds to the O-H stretching and bending vibration of H_2O in the nanofibers. The weak bands at 2926 cm^{-1} and 2917 cm^{-1} are assigned to C-H stretching frequency of sp^3 hybridized alkyl group. The CH_2 bending frequency has revealed at 1405 cm^{-1} , 1399 cm^{-1} and 1401 cm^{-1} . The weak bands observed at 1632 cm^{-1} , 1629 cm^{-1} and 1628 cm^{-1}

Table 1. Crystallite size, lattice strain and other parameters calculated from XRD images as a function of post annealing temperature

Peak number	Temperature [°C]	(h k l)	d [Å]	Lattice parameter [Å]	Crystallite size D [nm]	Stress [MPa]	Strain	Dislocation density [$10^{14} \times \text{m}^{-2}$]
1	400	2 0 0	2.317	a = 4.634	27.94	194.34	12.956	12.807
2		0 2 0	2.588	b = 5.177	34.48	157.47	10.498	8.408
3		0 0 2	2.528	c = 5.056	28.40	191.19	12.74	12.390
Average values					30.27	181.00	12.064	11.202
1	500	2 0 0	2.318	a = 4.635	27.94	194.34	12.95	12.807
2		0 2 0	2.220	b = 4.440	28.30	191.88	12.79	12.485
3		0 0 2	2.520	c = 5.040	28.40	191.19	12.74	12.390
Average values					28.21	192.47	12.826	12.561
1	600	2 0 0	2.319	a = 4.638	29.82	182.11	12.141	11.245
2		0 2 0	2.252	b = 5.035	28.93	187.66	12.511	11.942
3		0 0 2	2.521	c = 5.042	30.80	176.28	11.75	10.536
Average values					29.85	182.02	12.134	11.241

Table 2. EDX analysis of Zn-CuO nanofibers post-annealed at different temperatures.

Zn-CuO	Zn [wt.%]	Cu [wt.%]	Si [wt.%]	O [wt.%]
400 °C	51.89	26.20	–	21.91
500 °C	55.52	28.91	2.11	13.46
600 °C	58.19	27.01	3.5	11.30

correspond to the C=C stretching frequency. These weak peaks show the presence of impurities present on the surface of the metal oxide nanofibers. The band observed between 900 cm^{-1} and 1500 cm^{-1} corresponds to the oxygen stretching and bending frequencies [42, 43]. No characteristic peaks are observed at 453 cm^{-1} for ZnO formation [44] which confirms the formation of Zn doped CuO nanofibers.

The optical properties of the Zn-CuO nanofibers were recorded in the wavelength range of 200 nm to 800 nm (Fig. 6). Broad absorption peaks are observed around 261 nm, 263 nm and 267 nm for the samples of Zn-CuO post-annealed at 400 °C, 500 °C and 600 °C, respectively and the corresponding cut-off wavelength occurs at 344 nm, 351 nm and 353 nm. The weak bands for corresponding Zn-CuO nanofibers appear at 679 nm (400 °C), 676 nm (500 °C) and 692 nm (600 °C), respectively. The band gaps

of the post-annealed Zn-CuO nanofibers were calculated using the equation:

$$E = \frac{hc}{\lambda} \quad (3)$$

where h is the Planck constant, c is the velocity of light and λ is the wavelength of the UV-Vis spectrum.

The band gap energy changed due to the post annealing causing a change in the grain size of the Zn-CuO nanofibers respectively. From the observations, the band gap of the post-annealed Zn-CuO nanofibers increased with an increase in temperature. A blue shift was observed due to the quantum confinement of 1D nanostructured materials [45]. The calculated band gaps were found to be 1.86 eV, 1.94 eV and 1.98 eV at the post annealing temperatures of 400 °C, 500 °C and 600 °C. These results are consistent with the effective mass theory (EMA).

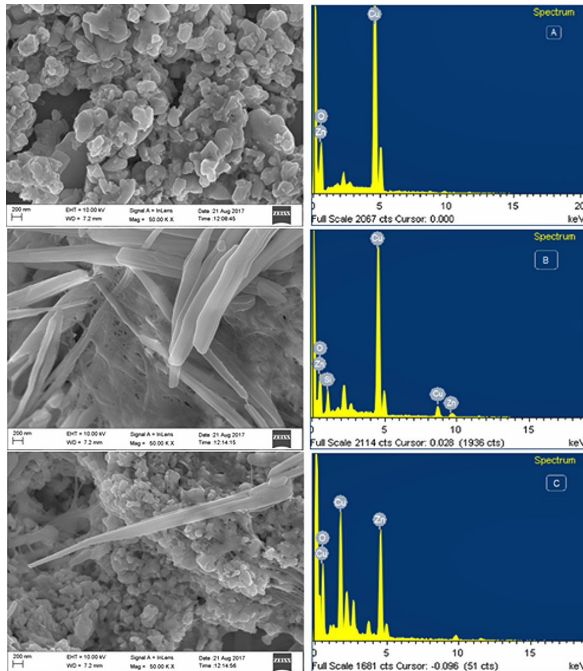


Fig. 4. SEM micrographs of Zn-CuO nanofibers along with their EDX analysis results: (a) Zn-CuO post-annealed at 400 °C; (b) Zn-CuO post-annealed at 500 °C; (c): Zn-CuO post-annealed at 600 °C.

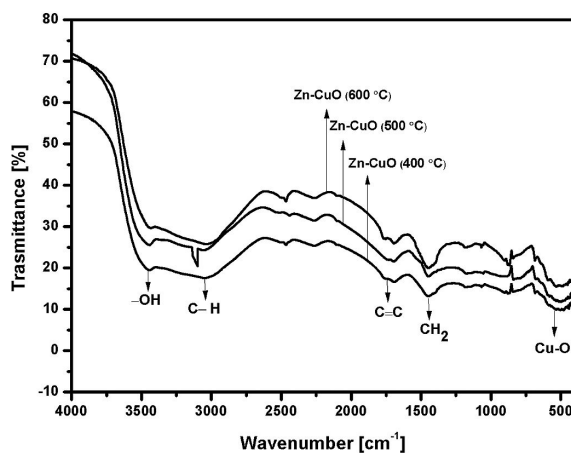


Fig. 5. FT-IR spectra of Zn-CuO nanofibers post-annealed at 400 °C, 500 °C and 600 °C.

3.2. Photocatalytic studies

The photocatalytic reaction was performed using the Zn-CuO nanofiber post-annealed at 500 °C, since it shows excellent properties deduced from the characterization analysis. The collector plate

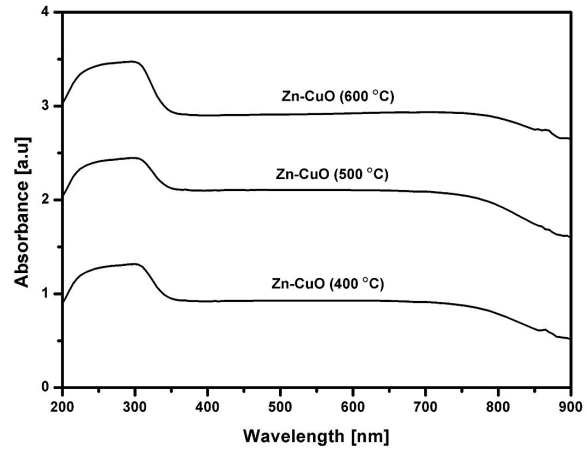


Fig. 6. UV-DRS spectra of Zn-CuO nanofibers post-annealed at 400 °C, 500 °C and 600 °C.

containing electrospun Zn-CuO nanofiber was suspended with the help of a holder inside the beaker containing 10 mg/L of methylene blue dye solution. The beaker was kept inside another vessel containing water flowing in and out continuously acting as a cooling chamber. The complete setup was placed upon a magnetic stirrer with a pellet placed inside the beaker containing the dye solution. A 125 V, high pressure mercury lamp was used as a source to enhance the photodegradation of the dye. The efficiency of the photodegradation of methylene blue dye using prepared Zn-CuO nanofiber was calculated with the absorbance measured using UV-Vis spectrophotometer (Shimadzu 3600) using the equation:

$$\text{Process efficiency [\%]} = \frac{C - C_o}{C} \times 100 \quad (4)$$

where C is the initial concentration and C_o is the concentration of methylene blue dye solution at time t (mg/L).

3.2.1. Process optimization

The photocatalytic degradation of methylene blue dye was carried out at pH ranging from 4 to 9, with initial methylene blue dye concentration of 10 mg/L to 50 mg/L for a period of 180 min at 30 min regular time intervals. The experimental observations of optimization of pH and initial dye concentration are presented in Fig. 7.

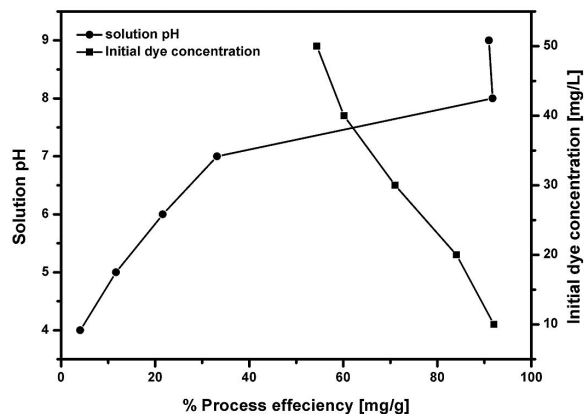


Fig. 7. Optimization of pH and initial dye concentration in methylene blue degradation process using Zn doped CuO nanofiber photocatalyst.

From the observations, it is clear that photodegradation efficiency is low at acidic pH but with gradual increase in pH, effective decolorization of the methylene blue dye was achieved at basic pH of 8. At basic pH, OH^- radicals shall combine with the holes present in the photocatalyst surface, generating more and more OH^- radicals. Since the OH^- radicals are the most dominating oxidizing species in the photodegradation process, higher degradation of MB dye takes place at the basic medium [46]. Rapid degradation takes place initially but with an increase in dye concentration, the photodegradation efficiency decreases gradually. This is mainly due to the availability of free electrons from the Zn-CuO photocatalyst. But with an increase in dye concentration, the overcrowding of dye molecules around the photocatalyst makes the electron-hole transfer slow, resulting in slow photodegradation.

The time period required for the maximum degradation of methylene blue dye using Zn-CuO nanofiber was analyzed and presented in Fig. 8.

The time period parameter optimization was carried out at $\text{pH} = 8$ in solution containing 10 mg/L of methylene blue dye. The photocatalytic experiment was conducted and solution was withdrawn at every 30 min time intervals, centrifuged (1000 rpm) and analyzed using UV-Vis spectrophotometer. A spectrum with a sharp peak

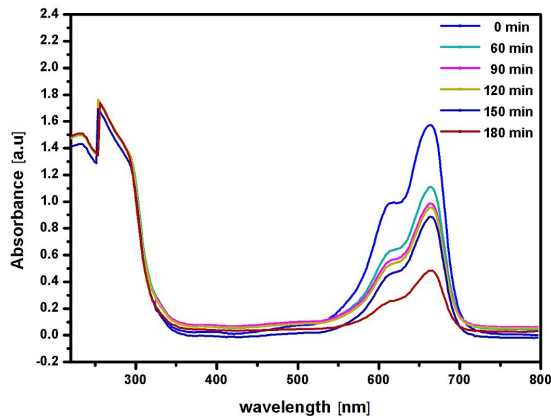


Fig. 8. Time period optimization of methylene blue degradation using Zn-CuO nanofiber.

at a wavelength of 664 nm was obtained. After every time interval, the intensity of the peak diminished, depicting the degradation of methylene blue dye. After 180 min, maximum degradation took place. The decrease in peak intensity was due to the interaction between the electrons generated by the Zn-CuO photocatalyst and the dye molecules present in the solution. Subsequent degradation of dye molecules was caused by the photocatalyst at a particular time, when no more dye molecules were available.

3.3. Photocatalytic kinetics

The photocatalytic activity of Zn doped CuO nanofiber was evaluated by calculating the rate of photodegradation of methylene blue dye. The light induced photodegradation of methylene blue dye follows first order kinetic model obeying Langmuir-Hinshelwood model [47, 48]. For better understanding of the photocatalytic reaction, kinetics of methylene blue dye degradation experiments were conducted. The degradation data were analyzed using pseudo-first order kinetic model [49] expressed by the equation:

$$-\ln \frac{C}{C_0} = kt \quad (5)$$

where C and C_0 represent the concentration of methylene blue dye solution at time zero and t , and k is the pseudo-first order rate constant. A plot of $-\ln(C/C_0)$ against time t is presented in Fig. 9.

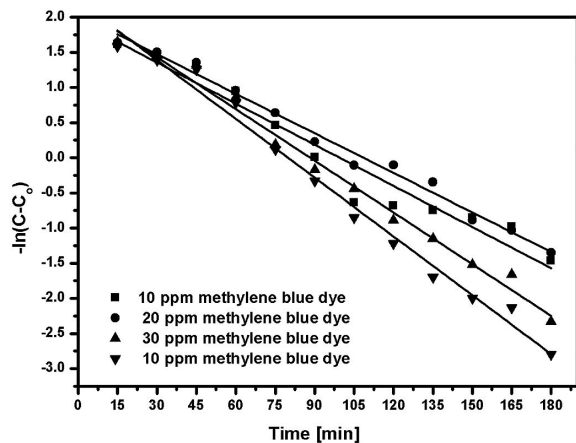


Fig. 9. Photodegradation kinetics of methylene blue dye using Zn-CuO nanofiber photocatalyst.

The values of rate constant and correlation coefficient (R^2) were calculated and presented in Table 3.

The effect of addition of Zn dopant into the CuO matrix resulted in the production of electron-hole pair and after reacting with sufficient amount of chemical elements, the hydroxyl group ions got converted into superoxy radicals $O_2^{\bullet-}$ and hydroxyl OH^\bullet radicals which effectively suppressed the recombination of electron-hole pairs. The excessive negative potential in the conduction band causes the electrons to reduce the molecular oxygen to superoxide radicals and the excessive positive potential present in the valence band causes the holes to directly react with the water to yield hydroxyl radicals or degrades the methylene blue dye directly. The hydroxide radicals have an ability to oxidize dye molecules or generate electron-hole pair [50].

3.4. Reusability test

The reusability test of the Zn-CuO nanofiber was performed to assess cost-effectiveness of the photodegradation system. For each experiment, the Zn-CuO photocatalyst was used with a freshly prepared methylene blue dye solution. The observations are presented in Fig. 10.

The Zn-CuO nanofiber was found to be stable up to four consecutive cycles and slowly lost its properties. This was due to the limited stability and slow oxidation potential

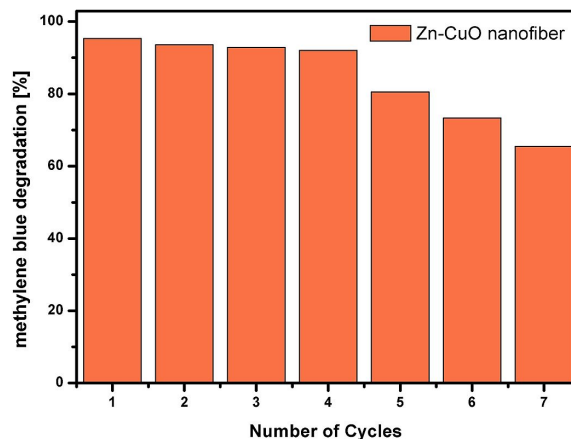


Fig. 10. Reusability studies of Zn-CuO nanofiber photocatalyst.

of the photocatalyst employed [51]. The reusability results showed the practical applicability of the Zn-CuO nanofiber which was found to be effective due to the molecular integrity of the co-doped sample and stability of the catalyst.

4. Conclusions

In summary, the Zn-CuO precursors post-annealed at different temperatures (400 °C, 500 °C and 600 °C) were electrospun onto nanofibers using the designed nanofiber generator. The effect of post-annealing temperature on the formation of nanofibers was analyzed. It was observed that the crystallite size of the nanofiber decreased with an increase in the post-annealing temperature. From the spectral characterization results it was stated that the incorporation of Zn^{2+} into CuO matrix resulted in the formation of spherically-shaped nanostructured material of 30 nm average crystallite size. The optical study showed that incorporation of Zn into CuO matrix caused an increase in the band gap, whose value raised also with an increase in the post-annealing temperature. A blue shift was observed in the absorption band, enhancing photocatalytic activity. The highly ordered Zn-CuO nanofiber was employed for the photocatalytic studies. Maximum methylene blue degradation was achieved with 10 ppm of methylene blue solution at pH 8 in 180 min. Reaction kinetics was employed to study the role of Zn-CuO nanofiber

Table 3. Kinetic parameters of Zn-CuO nanofiber used for the photodegradation of methylene blue dye

Sample	Methylene blue concentration [ppm]	K [min^{-1}]	R ²
Zn-CuO (500 °C)	10	0.3319	0.9905
	20	0.2987	0.9635
	30	0.3176	0.9918
	40	0.3028	0.9785

as a photocatalyst for effective photodegradation process. Reusability test was performed and stability up to four consecutive cycles was found. To sum up, we have fabricated Zn-CuO nanofibers which can be effectively used in environmental applications.

Acknowledgements

The authors would like to express their sincere thanks to Dr. S.R.K. Prasad (Correspondent, CIT), Dr. R. Prabhakar (Secretary, CIT), Dr. V. Selladurai (Principal, CIT), Mr. S. Rajiv Rangasamy (Director, CIT), Correspondent of KCT, Secretary of KCT and Principal of KCT for their help and encouragement during work.

References

- [1] KAURA M., MUTHEA K.P., DESPANDEB S.K., CHOUDHURY C.S., SINGHD J.B., VERMAE N., GUP-TAA S.K., YAKHMIA J.V., *J. Cryst. Growth*, 289 (2006), 670.
- [2] GAO X.P., BAO J.L., PAN G.L., ZHU H.Y., HUANG P.X., WU F., SONG D.Y., *J. Phys. Chem. B*, 108 (2004), 5547.
- [3] WANG S.Q., ZHANG J.Y., CHEN C.H., *Scripta Mater.*, 57 (2007), 337.
- [4] LI J.Y., XIONG S.L., XI B.J., LI X.G., QIAN Y.T., *Cryst. Growth Des.*, 9 (2009), 4108.
- [5] VASEEM M., UMAR A., HAHN Y.B., KIM D.H., LEE K.S., JANG J.S., LEE J.S., *Catal. Commun.*, 10 (2008), 11.
- [6] XU Y., CHEN D., JIAO X., *J. Phys. Chem. B*, 109 (2005), 13561.
- [7] AL-AMRI S., ANSARI M.S., RAFIQUE S., ALD-HAHRI M., RAHIMUDDIN S., AZAM A., MEMIC A., *Curr. Nanosci.*, 11 (2015), 191.
- [8] JAN T., IQBAL J., MANSOOR Q., ISMAIL M., NAQVI S.H., GUL A., NAQVI S.F.H., ABBAS F., *J. Phys. D Appl. Phys.*, 47 (2014), 355301.
- [9] IQBAL J., JAN T., UL-HASSAN S., AHMED I., MANSOOR Q., ALI M.U., ABBAS F., ISMAIL M., *AIP Adv.*, 5 (2015), 127112.
- [10] XI Y., HU C., GAO P., YANG R., HE X., WANG X., WAN B., *Mater. Sci. Eng. B-Adv.*, 166 (2009), 113.
- [11] SAHAY R., SUNDARAMURTHY J., KUMAR P.S., THAVASI V., MHAISALKAR S.G., RAMAKRISHNA S., *J. Solid State Chem.*, 186 (2012), 261.
- [12] DAR M.A., KIM Y.S., KIM W.B., SOHN J.M., SHIN H.S., *Appl. Surf. Sci.*, 254 (2008), 7477.
- [13] CHEN L., SHET S., TANG H.W., WANG H.L., DEUTSCH T., YAN Y.F., TURNER J., ALJASSIM M., *J. Mater. Chem.*, 20 (2010), 6962.
- [14] RAY S.C., *Sol. Energ. Mat. Sol. C.*, 68 (2001) 307.
- [15] MARUYAMA T., *Sol. Energ. Mat. Sol. C.*, 56 (1998) 85.
- [16] RENEKER D.H., YARIN A.L., *Polymer*, 49 (2008) 2387.
- [17] KUMAR P.S., ABHINAYA R.V., ARTHI V., GAYATHRI-LASHMI K., PRIYADHARSHINI M., SIVANESAN S., *Environ. Eng. Manag. J.*, 13 (2014) 545.
- [18] VIDHYADEVI T., MURUGESAN A., KALAIVANI S.S., PREMKUMAR M.P., KUMAR V.V., RAVIKUMAR L.R., SIVANESAN S., *Desal. Water Treat.*, 52 (2014) 19.
- [19] VIDHYADEVI T., MURUGESAN A., KALAIVANI S.S., PREMKUMAR M.P., RAVIKUMAR L., SIVANESAN S., *Korean J. Chem. Eng.*, 32 (2015) 650.
- [20] SENTHAMARAI C., KUMAR P.S., PRIYADHARSHINI M., VIJAYALAKSHMI P., KUMAR V.V., BASKARALINGAM P., THIRUVENGADARAVI K.V., SIVANESAN S., *Environ. Prog. Sustain. Energ.*, 32 (2013) 624.
- [21] KUMAR P.S., RAMALINGAM S., SATHYASELVABALA V., KIRUPHA S.D., SIVANESAN S., *Desalination*, 266 (2011) 63.
- [22] KUMAR P.S., SATHYASELVABALA V., RAMAKRISHNAN K., VIJAYALAKSHMI P., SIVANESAN S., *Russ. Chem. Bull.*, 59 (2010) 1859.
- [23] KUMAR P.S., RAMALINGAM S., KIRUPHA S.D., MURUGESAN A., VIDHYADEVI T., SIVANESAN S., *Chem. Eng. J.*, 167 (2011) 122.
- [24] KUMAR P.S., SATHYASELVABALA V., KIRUPHA S.D., VIJAYALAKSHMI P., SIVANESAN S., *Environ. Eng. Manag. J.*, 10 (2011) 285.
- [25] KUMAR P.S., RAMALINGAM S., ABHINAYA V., THIRUVENGADARAVI K.V., BASKARALINGAM P., SIVANESAN S., *Sep. Sci. Technol.*, 46 (2011) 2436.
- [26] KUMAR P.S., RAMALINGAM S., ABHINAYA V., KIRUPHA S.D., VIDHYADEVI T., SIVANESAN S., *Can. J. Chem. Eng.*, 90 (2012) 973.
- [27] KUMAR P.S., RAMALINGAM S., ABHINAYA R.V., KIRUPHA S.D., MURUGESAN A., SIVANESAN S., *Clean*, 40 (2012) 188.
- [28] KUMAR P.S., RAMALINGAM S., SATHYASELVABALA V., KIRUPHA S.D., MURUGESAN A., SIVANESAN S., *Korean J. Chem. Eng.*, 29 (2012) 756.

- [29] RAJKUMAR P., KUMAR P.S., KIRUPHA S.D., VIDHYADEVI T., NANDAGOPAL J., SIVANESAN S., *Environ. Prog. Sustain. Energ.*, 32 (2013) 307.
- [30] KUMAR P.S., SENTHAMARAI C., DURGADEVI A., *Environ. Prog. Sustain. Energ.*, 33 (2014) 28.
- [31] KUMAR P.S., SENTHAMARAI C., SAI DEEPTHI A.S.L., BHARANI R., *Can. J. Chem. Eng.*, 91 (2013) 1950.
- [32] SARAVANAN A., KUMAR P.S., YASHWANTHRAJ M., *Desal. Water Treat.*, 68 (2017) 245.
- [33] KUMAR P.S., VARJANI S.J., SUGANYA S., *Bioresour. Technol.*, 250 (2018) 716.
- [34] SARAVANAN A., KUMAR P.S., RAJAN P.S.S., ABISHEK S., ABHISHEK D., *Korean J. Chem. Eng.*, 33 (2016) 2716.
- [35] CAROLIN C.F., SARAVANAN A., KUMAR P.S., RAJAN P.S., KUMAR V.V., *IET Nanobiotechnol.*, 11 (2017) 433.
- [36] CAROLIN C.F., KUMAR P.S., SARAVANAN A., JOSHIBA G.J., NAUSHAD M., *J. Environ. Chem. Eng.*, 5 (2017) 2782.
- [37] XU L., ZHOU Y., WU Z., ZHENG G., HE J., ZHOU Y., *J. Phys. Chem. Solids*, 106 (2017), 29.
- [38] GUNASUNDARI E., KUMAR P.S., *J. Ind. Eng. Chem.*, 56 (2017) 129.
- [39] SARAVANAN A., KUMAR P.S., RENITA A.A., *J. Clean. Prod.*, 172 (2018) 92.
- [40] KUMAR P.S., PALANIYAPPAN M., PRIYADHARSHINI M., VIGNESH A.M., THANJIAPPAN A., FERNANDO P.S.A., AHMED R.T., SRINATHA R., *Environ. Prog. Sustain. Energ.*, 33 (2014) 87.
- [41] SARAVANAN R., KARTHIKEYAN S., GUPTA V.K., SEKARAN G., NARAYANAN V., STEPHEN A., *Mater. Sci. Eng. C*, 33 (2013), 91.
- [42] ZHU J.W., LI D., YANG X.J., LU L.D., WANG X., *Mater. Lett.*, 58 (2004), 3324.
- [43] HAMMAD T.M., SALEM J.K., HARRISON R.G., *Rev. Adv. Mater. Sci.*, 22 (2009), 74.
- [44] ODA A.M., ALI H.H., LAFTA A.J., ESMAEL H.A., JAMEEL A.A., MOHAMMED A.M., MUBARAK I.J., *Int. J. Chem.*, 7 (2015), 39.
- [45] SAHAY R., SUNDARAMURTHY J., KUMAR P.S., THAVASI V., MHAISALKAR S.G., RAMAKRISHNA S., *J. Solid State Chem.*, 186 (2012) 261.
- [46] PITCHAIMUTHU S., RAJALAKSHMI S., KANNAN N., VELUSAMY P., *Desalin. Water Treat.*, 52 (2014), 3392.
- [47] BAYATI M.R., GOLESTANI-FARD F., MOSHFEGH A.Z., *Appl. Surf. Sci.*, 256 (2010) 4253.
- [48] BECHAMBI O., JLAIEL L., NAJJAR W., SAYADI S., *Mater. Chem. Phys.*, 173 (2016) 95.
- [49] NASERI A., SAMADI M., MAHMOODI N.M., POURJAVADI A., MEHDIPOUR H., MOSHFEGH A.Z., *J. Phys. Chem. C*, 121 (2017) 3327.
- [50] ESWARAN K., SIVARAMAN S., KAVITHA B., PREMA E.M., RAJARAJAN M., PARK S., *Appl. Surf. Sci.*, 433 (2018) 216.
- [51] ARUNADEVI R., KAVITHA B., RAJARAJAN M., SUGANTHI A., JEYAMURUGAN A., *Surf. Interface*, 10 (2018) 32.

Received 2018-03-13
Accepted 2018-04-06